Journal Name

ARTICLE TYPE

Cite this: DOI: 10.1039/xxxxxxxxxx

Role of size polydispersity in magnetic fluid hyperthermia: average vs. local infra/over-heating effects

Cristina Munoz-Menendez,*[a] Ivan Conde-Leboran,[a] Daniel Baldomir,[a] Oksana Chubykalo-Fesenko,[b] and David Serantes*[a,c,d]

Received Date
Accepted Date

DOI: 10.1039/xxxxxxxxxx

www.rsc.org/journalname

An efficient and safe hyperthermia cancer treatment requires the accurate control of the magnetic nanoparticles' heating performance, which is directly related to their size. However, in any particle system it is experimentally unavoidable the existence of some size polydispersity, what will result in a different *local* heating output and consequently a different hyperthermia performance depending on the size of each particle. Aiming to shed some light on this significant issue, we have used a Monte Carlo technique to study the role of size polydispersity in the heat dissipation at both the *local* (single particle) and *global* (macroscopic average) levels. We have systematically varied size polydispersity, temperature and interparticle dipolar interaction conditions; and evaluated the local heating as a function of those parameters. Our results provide a simple guide on how to choose, for a given polydispersity degree, the more adequate average particle size so that the *local* variation in the released heat is kept within some limits that correspond to safety boundaries for the average-system hyperthermia performance. All together we believe that our results may help in the design of more effective magnetic hyperthermia applications.

Magnetic fluid hyperthermia is a new medical technique for cancer treatment that aims to damage/destroy cancerous cells by increasing their temperature up to 41-46 °C.[1–4] The procedure consists in selectively targeting the tumor with magnetic nanoparticles (MNPs) and heating them up under an external AC magnetic field, thus increasing the temperature of the embedding media as illustrated in Fig. 1(a). The key-point is to control their heating performance so that the temperature rises enough as to harm the cancer cells while maintained within safety limits for the patient. An important advantage of this technique is the avoidance of the harmful *whole-body* secondary effects of the usual chemo/radiotherapies.

Several important issues need to be addressed in order to develop an efficient magnetic hyperthermia protocol for broad clinical use. Besides biological aspects as biocompatibility[5–7] and toxicity[7–10], the main problem is to achieve an accurate control of the heating performance of the particles. The dissipated heat strongly varies depending simultaneously on both the specific particle characteristics (anisotropy, volume, magnetization) and the

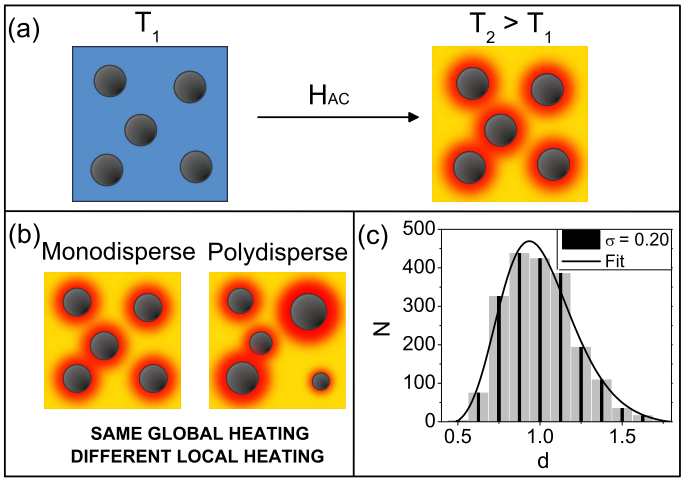

Fig. 1 (a) When an alternating magnetic field H_{AC} is applied, the system temperature increases from T_1 to T_2 as the particles release energy. (b) Scheme illustrating that apparently similar overall (global) heating of a monodisperse and a polydisperse system may have, however, completely different local heating profiles. (c) Lognormal distribution (solid line) of particle normalized diameters d assumed in the simulations, in this case for a degree of polydispersity $\sigma = 0.20$, to illustrate the discrete size categories -bars and black vertical lines in the middle.

[a] *Instituto de Investigacións Tecnolóxicas and Departamento de Física Aplicada, Universidade de Santiago de Compostela, 15782 Santiago de Compostela, Spain.*
[b] *Instituto de Ciencia de Materiales de Madrid, CSIC, Cantoblanco, ES-28049 Madrid, Spain.*
[c] *UCCS Biofrontiers Center, University of Colorado Colorado Springs, Colorado Springs, CO 80918, USA.*
[d] *Department of Physics, University of York, York YO10 5DD, U.K.*
* Corresponding authors: cristina.munoz@usc.es and david.serantes@usc.es

chosen experimental conditions (temperature, amplitude and frequency of the applied field, dose).[11–13] Intense research is currently being conducted to address those issues; for recent reviews see for example Refs. 1,2.

The objective of the present work is to investigate an essentially untackled aspect of the hyperthermia performance of magnetic nanoparticles: the role of size polydispersity, relating the heating at the *local* (heat dissipated by each particle) and the *global* (average) levels. Many works have investigated how polydispersity influences the hyperthermia performance of MNPs,[14–19] although mostly from the *global* point of view, i.e., the average properties of the entire system. Under this approach, in the literature it is usually reported a detrimental influence of size polydispersity on the heating power, ranging from moderate[20] to high[21]. Experimentally, the dissipated energy can drop between 30% and 50% for a degree of size polydispersity varying between $\sigma = 0.20$ and $\sigma = 0.25$.[22,23] However, it is worth noting that also the opposite trend, enhancement of the heating performance with higher polydispersity, has been described.[24]

The importance of investigating the heat dissipation at the local level is emphasized by some recent works reporting cell death by MNPs under an AC field without noticeable global (macroscopic) temperature rise.[25–28] These results raised some debate in the specialized literature concerning the usually presumed need to achieve a homogeneous temperature rise within the tumor as a key issue for an effective hyperthermia.[1,2,29,30] A possible explanation could be that even a localized temperature increment, occurring only at the nanoenvironment of the nanoparticles, could be enough to induce cells' apoptose without a significant global temperature increment. This interpretation seems to be supported by recent measurements indicating that the temperature difference attained during a hyperthermia experiment between the particle surface and its surroundings decreases abruptly, being negligible at just a few *nm* away from the nanoparticle surface.[31–33] Therefore, it could be possible to have sufficient *local* temperature enhancement to harm the cancer cells without a *global* temperature increment. Nonetheless, this is still an open question out of the scope of this work. Regarding the objective of the present study, those results[25–28] clearly support that studying the influence of polydispersity at local level merits exhaustive research.

Experiments generally report lognormal size distributions[15,18,34–38] -see Fig. 1(c)- with σ, the standard deviation of the logarithm of the diameter D of the particles, ranging between 0.10 to 0.25. A system with $\sigma \approx 0.10$ is already considered as monodisperse. Such polydispersity gives rise to a distribution of local heat-dissipation spots with different effect on the surrounding *nanoenvironment* (embedding cell or intercellular media). This is illustrated in Fig. 1(b), where two systems with apparently the same macroscopic (global) temperature correspond, however, to completely different *local* temperature nanoenvironments depending on the particle sizes. On the one hand, particles with poor heating performance might not reach the treatment temperature, leaving malignant cells alive. On the other hand, particles heating in excess could cause ablation, with the consequent risk of bleeding or infection.[39] To the best of our knowledge, no in-depth study has been done on how size polydispersity results in a distribution of locally different hyperthermia performance.

The work is organized as follows. In Section 1 we describe the physical model and the computational procedure. The use of numerical simulations is strongly justified due to the complexity of the objective and the need to have access to the information of the system properties at different levels: average heating of the entire system *vs.* heating of individual particles depending on their sizes. In Section 2 we present and discuss the results of the work. In Subsection 2.1, we study the influence of size polydispersity on the hyperthermia properties of the entire system in the non-interacting case. In Subsection 2.2 we investigate the role of polydispersity at a local level, introducing the evaluation of the local heating and its dispersion as significant parameters for hyperthermia characterization. In Subsection 2.3, the role of interparticle dipolar interactions is taken into account. Finally, the conclusions of the work are summarized in Section 3.

1 Model

The hyperthermia properties of MNPs are usually reported in terms of the *Specific Absorption Rate*, SAR, defined as $SAR = HL \cdot f$, with HL the hysteresis losses and f the frequency of the AC field. To study the role of polydispersity and interactions on the heating performance of the particles, we use a Monte Carlo method[37,40,41] to simulate magnetization (M) *vs.* field (H) hysteresis loops under different conditions (temperature, polydispersity degree, and interparticle coupling strength) and evaluate the HL values as the area of the loops.

In our model the spatial positions of the particles follow a liquid-like distribution resembling a frozen ferrofluid. This corresponds to conditions in which the nanoparticles are completely fixed into the tumor, that is to say, the contribution of the Brownian reversal to the heat dissipation is neglected. This assumption is in agreement with experimental works reporting a negligible influence[42] and even a total inhibition[43] of Brownian relaxation in cell-like conditions for hyperthermia applications. For an insightful work considering the dynamics of a particle in a viscous liquid see e.g. the work by Usov and Liubimov,[44] where the authors consider the simultaneous rotation of the particle as well as the jump of its magnetization over the anisotropy barrier.

The physical model corresponds to a polydisperse system of N single-domain magnetic nanoparticles with uniaxial magnetic anisotropy K and random easy axes distribution. For the sake of generality, from now on we will present the results in terms of the dimensionless normalized diameter $d = D/D_0$, being D_0 the diameter of the ideal monodisperse system. The average diameter of polydisperse systems $\langle D \rangle$ is kept equal to this value, i.e. $\langle D \rangle = D_0$. Following experimental observations, the size distribution is assumed to be lognormal[15,18,34–38] -see Figure 1(c)- and it is given by

$$f(d;u,\sigma) = \frac{1}{\sqrt{2\pi}d\sigma} e^{-\frac{(\ln(d)-u)^2}{2\sigma^2}}, \qquad (1)$$

where σ is the standard deviation of $\ln(d)$ and u is the average of the logarithms of the diameter. The atomic magnetic moments of each i-particle are assumed to rotate coherently, so that the

particles are characterized by their total *supermoment* $|\vec{\mu}_i| = M_S V_i$, where V_i is the particle volume and M_S is the saturation magnetization per volume. For simplicity, K and M_S are taken as size- and temperature-independent. The energies governing the magnetic response are the uniaxial anisotropy $E_A^{(i)} = -KV_i(\vec{\mu}_i \cdot \hat{n}_i/|\vec{\mu}_i|)^2$, being $\hat{n}$ the unitary vector along the easy axis; Zeeman, $E_Z^{(i)} = -\vec{\mu}_i \cdot \vec{H}$; and the dipolar interaction. The latter energy for two particles i, j is given by $E_D^{(ij)} = \vec{\mu}_i \cdot \vec{\mu}_j / r_{ij}^3 - (\vec{\mu}_i \cdot \vec{r}_{ij})(\vec{\mu}_j \cdot \vec{r}_{ij})/r_{ij}^5$, being $\vec{r}_i$, $\vec{r}_j$ the i,j-particle positions and $\vec{r}_{ij}$ the vector connecting them.

The total magnetization of the N-particle system along the field direction is $M = \sum_{i=1}^{N} M_S V_i cos\theta_i$, being θ_i the angle between $\vec{\mu}_i$ and $\vec{H}$. The M *vs.* H hysteresis loops are reported in dimensionless units as $M/M_S V_t^0$ and $h = H/H_A$ respectively, where $V_t^0 = NV_0$ is the total volume of the monodisperse system, V_0 the volume of one of its particles and $H_A = 2K/M_S$ is the anisotropy field. The temperature is also treated in normalized units as $t = k_B T/2KV_0$, in terms of the anisotropy energy barrier of the non-interacting monodisperse particles KV_0.

A system of $N = 2000$ particles was considered in all the simulations and the field amplitude H_{max} was always set as $h_{max} = 5$, well above the saturation field of the particles in order to avoid complicated minor-loop considerations[40] and ease the understanding of the results. We have adjusted the number of Monte Carlo steps to coincide with the Stoner-Wohlfarth results (with coercive field $H_C \approx 0.48 H_A$ and the remanence $M_R \approx 0.5 M_S V_t^0$) for the monodisperse case at very low temperature and for a non-interacting ensemble. These conditions also determine the maximum achievable power, $HL_{max}^0 = 2KV_t^0$ for the monodisperse system. Since we are working in reduced units, from now one we will use $hl = HL/HL_{max}^0$ to refer to the reduced hysteresis losses, so in this case we will write $hl_{max}^0 = 1$. For the polydisperse system one has $HL_{max} = 2KV_t$ where V_t is the total volume of the polydisperse system.

We assumed a discrete particle size distribution so that the particles of the system can be grouped within a finite set of size categories. The maximum number of categories (P) considered in this work for all polydispersity conditions is $P = 25$, with N_j particles in each j-category. The total magnetization M may be normalized and rewritten in terms of the different size categories as

$$\frac{M}{V_t^0 M_S} = \frac{1}{N}\sum_{i=1}^{N} v_i cos\theta_i = \frac{1}{N}\sum_{j=1}^{P} N_j \mathscr{M}_j, \qquad (2)$$

where $v_i = \frac{V_i}{V_0}$ is the reduced volume of the particle i and $\mathscr{M}_j$ is the magnetization of each j-category. $\mathscr{M}_j$ is given by

$$\mathscr{M}_j = \frac{v_j}{N_j}\sum_{k=1}^{N_j} cos\theta_{kj}. \qquad (3)$$

Accordingly, the magnetization of each category with volume v_j will vary between $-v_j$ and $+v_j$, as illustrated in Fig. 3. This way of presenting the results will allow the direct estimation of the hysteresis losses of each category, $(hl)_j$, in relation to the hysteresis losses of the monodisperse system. Note that at low temperatures the coercive field of each category is the same. This situation will be different with increasing temperature, when the thermal fluctuations will progressively become comparable to the anisotropy energy barriers of the smaller particles.

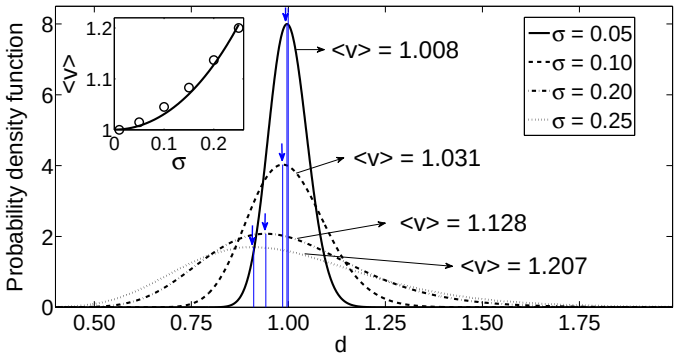

Fig. 2 Lognormal distributions of samples with different standard deviation σ but the same average diameter. The mean volume $\langle v \rangle$ increases and the most probable value (mode) decreases with rising polydispersity. Inset: Evolution of $\langle v \rangle$ with σ.

2 Results and discussion

2.1 Influence of polydispersity on the entire system in the non-interacting case

To compare the hysteresis losses of polydisperse samples having different σ with the ones of the monodisperse system, we normalize $HL_{max}/HL_{max}^0 = V_t/V_t^0 = V_t/(NV_0) = \langle V \rangle/V_0$ where $\langle V \rangle$ is the average volume of the system. In dimensionless units, $hl_{max} = \langle v \rangle$, where $\langle v \rangle = \langle V \rangle/V_0$.

It is important to correlate the properties of the lognormal distribution in diameters with those in volumes. In general it is known that for a continuous distribution with probability density function $f(x)$, the expected value of x^n is the n-*th* (raw) moment $E(x^n) = \int x^n f(x)dx$, $n \in \aleph$. For the lognormal distribution we have

$$E(x^n) = e^{\left\{nu + \frac{1}{2}n^2\sigma^2\right\}}. \qquad (4)$$

From Eq.4 we obtain $\langle v \rangle = e^{3u + \frac{9}{2}\sigma^2}$. For the comparison among different samples with the same average diameter and different polydispersity it is more convenient to rewrite this equation in terms of $\langle d \rangle$ as $\langle v \rangle = e^{3\left(\ln\langle d \rangle + \sigma^2\right)}$. Thereby, we obtain that the normalized average volume $\langle v \rangle$ for any particle distribution with a constant $\langle d \rangle$ value depends on σ as

$$\langle v \rangle = e^{3\sigma^2}. \qquad (5)$$

The above Eq.5 provides a useful insight into the influence of polydispersity on the *global* hysteresis losses in a non-interacting system. Since $hl_{max} \approx \langle v \rangle$, it predicts an increase of the hysteresis losses with increasing σ for a fixed $\langle d \rangle$ for low temperatures. This influence of polydispersity is illustrated in figure 2, where it is seen that $\langle v \rangle$ increases when broadening the distribution. Interestingly, the most probable value -i.e. the peak of the distribution-, decreases with increasing σ. The inset of figure 2 shows that the $\langle v \rangle$ values used in our simulations (open circles), which were defined independently to follow a lognormal distribution in diameters, are consistent with Eq.5.

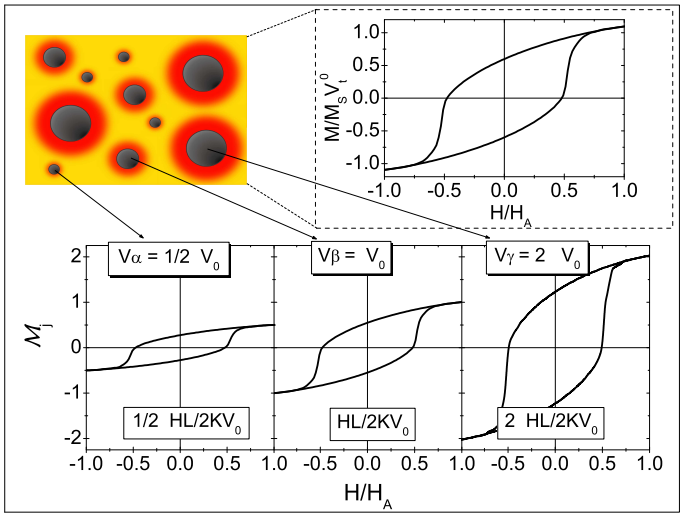

Fig. 3 Influence of the particle size on the *local* reduced hysteresis losses. The upper panel depicts the usual hysteresis curve of the entire system. In the lower panels some examples of the hysteresis loops corresponding to different sizes are shown in terms of the magnetization of each category $\mathscr{M}_j$. Three different cases are considered: the same as the mean volume of the monodisperse system ($V_\beta = V_0$), a smaller one ($V_\alpha = V_0/2$) and a bigger one ($V_\gamma = 2V_0$). The expected different heating performance is clearly observed.

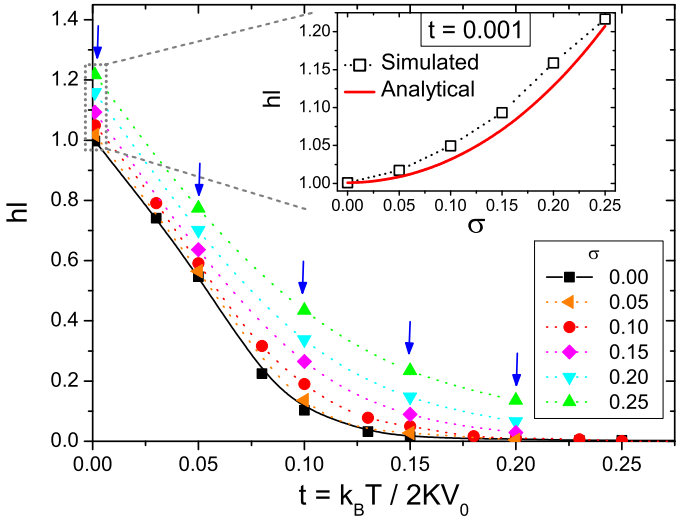

Fig. 4 Temperature dependence of the global reduced hysteresis losses hl for different degrees of polydispersity σ. Blue arrows indicate the chosen reduced temperatures to perform a systematic study of the system properties. The inset shows the comparison between the hl obtained from the simulations and the prediction of Eq.5.

The simulated dependence of hysteresis losses on temperature is shown in Fig. 4, where a decrease of the hl with increasing t is observed, in agreement with experimental results.[45] This behavior is due to the increased probability of the magnetization jump over the anisotropy barrier with increasing temperature. The inset shows that at very low t the dependence of the hl value on σ follows well the predictions of Eq.5. We attribute the slight deviation to the difference between the exact lognormal distribution of the analytical expression and the approximated discrete distribution of the simulations.

From Fig. 4 we can conclude that polydispersity has a moderate influence on the hl at low t, in agreement with previous results reported in the literature.[20] However, the opposite occurs at high t, with noticeable hl values in the polydisperse system even at temperatures at which the losses of the monodisperse system become negligible. This behavior is easily explained by the increasing fraction of particles that, with larger σ, exhibits blocked behavior at temperatures at which the monodisperse sample would behave superparamagnetically (i.e. dissipationless). A similar interpretation is reported in Ref. 18.

It is important to recall here that our simulations always predict an increase of hl with polydispersity. This has been also previously seen, for example, in Ref. 24. However, also the opposite trend, i.e. polydispersity being detrimental to heating performance, has been reported in the literature.[22,23] We attribute such apparent contradiction to an insufficient H_{max} value to reverse the magnetization of the particles[40] (minor-cycle conditions, while our simulations correspond to major-cycle conditions). Indeed, if a fraction of the system corresponds to minor-cycle conditions, a larger σ will progressively increase the fraction of particles that do not switch. Since these particles are the largest with a more important contribution to heating, this may result in lowering the heating output. Experimental results supporting our interpretation are those reported in Refs. 24 and 23: in Ref. 24, $H_{max} \gg H_A$ (major cycles) for both $MgFe_2O_4$ and $NiFe_2O_4$ particles and hysteresis losses increase with size polydispersity. On the contrary, in Ref. 23, $H_{max} \approx H_A$ (Fe_3O_4 MNPs) and the heating performance decreases with σ. Note that the role of interparticle interactions as the origin of the increasing hysteresis losses envisaged by the authors of Ref. 24 does not contradict our results, which always predict, no matter the interaction conditions, an increase of the released energy with rising σ. In addition, it is important to note that this major/minor cycle condition is presumably not enough, just by itself, to explain the complex behavior of magnetic nanoparticle systems, with a complicated entwined dependence on particle parameters and experimental conditions[11,46].Therefore, an extensive study of the hyperthermia properties as a function of H_{max} needs to be performed in order to gain further understanding on the role of field-dependence on the global/local hyperthermia properties. Such study lays, however, out of the scope of the present work. Furthermore, experimentally we can also expect to have polydispersity in the values of anisotropy that will play a role at two different levels: in addition to the same influence as the volume regarding stability against thermal fluctuations, having different K-values will play a central role in relation to the achievable H_{max}/H_A value that also determines the heating performance.[40] For an insightful discussion in this regard, see e.g. the work by Vallejo-Fernandez *et al.*[47]

2.2 Role of polydispersity at local level in the non-interacting case

Using Eq. 2 we examine the hysteresis losses for the different particle sizes. Some illustrative results are shown in Fig. 3 where we underly that larger particles dissipate more energy than the

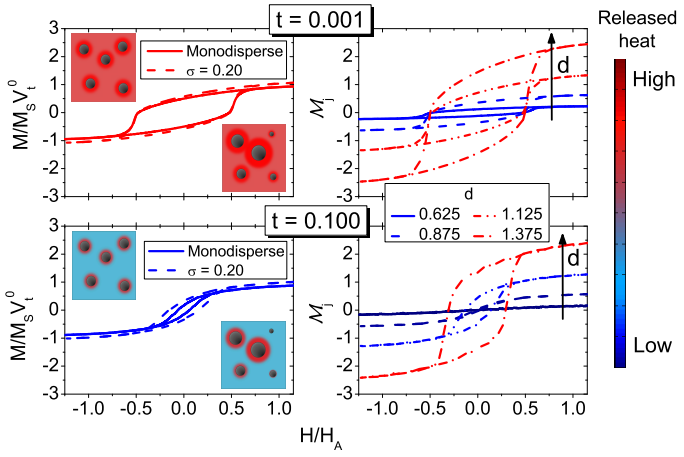

Fig. 5 (Color online) Comparison between a monodisperse and a polydisperse system at two different reduced temperatures, $t = 0.001$ (top panels) and $t = 0.100$ (lower panels). For each t the left panel shows the average hysteresis cycles of the entire system, whereas the right panels stand for the hysteresis cycles of different particle sizes.

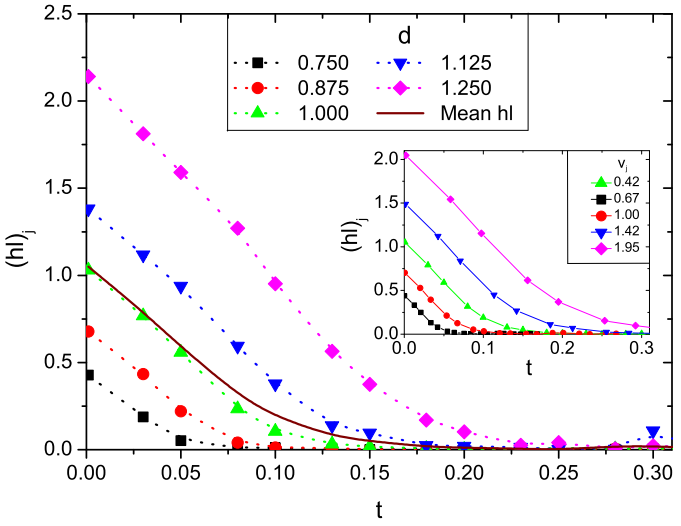

Fig. 6 Evolution of the hysteresis losses (per particle) $(hl)_j$ for the different size categories of a particle system with $\sigma = 0.10$. The solid line stands for the mean reduced hysteresis losses evaluated from the area of the global hysteresis loop hl. The inset shows the rescaled hysteresis losses obtained from the global curve.

smaller ones. The same is illustrated in Fig. 5 as a function of temperature, where a polydisperse system is compared with the ideal monodisperse one. The results indicate that while at low t there is not much difference between the monodisperse and the polydisperse samples, a different trend is observed at higher t. The separated contributions to hl (right panels) explains such differences between low and high temperature. At low t all particles contribute to heating. On the contrary, at high t the hysteresis loops of the smaller particles become anhysteretic and therefore only the larger particles contribute to heat dissipation.

Fig. 6 shows the systematic evaluation of the hl of each category as a function of t for $\sigma = 0.10$. As expected, the bigger is the particle size, the larger is its contribution to heat dissipation and its robustness against thermal fluctuations. Noteworthy, the shape of the curves is very similar for the different sizes. This could be anticipated if considering that, for non-interacting conditions, the different curves may be obtained by rescaling the results corresponding to just one particle size. This is illustrated in the inset of Fig. 6, since $hl \propto \langle v \rangle$ one can approximately obtain all category curves from the mean hysteresis losses of the entire system. This supports the suitability of assessing the local heating capability of the different particle sizes from their respective hysteresis loops, as described at the beginning of Section 2. This supports the suitability of assessing the local heating capability of the different particle sizes from their respective hysteresis loops, as described at the beginning of Section 2. The slight deviations between the main panel and the inset are explained by the existence of very small particle sizes with decreased heating contribution in the simulated system that lower the overall hysteresis losses.

We next address the dispersion in local heating in relation to the size polydispersity and temperature. This is characterized by means of the standard deviation s_{hl}. We have performed this evaluation for the 5 different reduced temperatures indicated in Fig. 4 (vertical arrows) and for $\sigma = 0.05$, 0.10, 0.15, 0.20 and 0.25. The s_{hl} value is defined as:

$$s_{hl} = \sqrt{\frac{1}{N}\sum_{j=1}^{P} N_j \left[(hl)_j - \langle (hl)_j \rangle \right]^2}. \qquad (6)$$

The s_{hl} values corresponding to the data reported in Fig. 4 are displayed in Fig. 7, where we observe a rapid increase of s_{hl} with larger σ but an overall decrease with increasing t. Therefore, the preference of having a monodisperse sample in order to have homogeneously released heat into the tumor [1,2,29] is stressed once again.

Importantly, Fig. 7 may serve as a tool to define safety boundaries for the dispersion in the performance of the local heat dissipation spots. Remembering that $t = k_B T/2KV_0$ and assuming that our synthesis technique allows a certain σ, Fig. 7 shows how to choose the particle volume for a given T so that σ_{hl} is kept below a desired value. For example, in Fig. 7 we see that for having σ_{hl} under the 30% depicted by the horizontal line, larger particles can be used for $\sigma = 0.10$ than for $\sigma = 0.20$. Thus, for a given σ, the way of lowering the dispersion in the local performance is by reducing the particle size, with the consequent drawback of diminishing the heating output. It has to be noted that this predictions hold for saturated cycles, being necessary further investigation to disclose what happens for minor loops. Therefore, the design of a hyperthermia protocol considering a clinically acceptable local dispersion in heat dissipation will require to put together the results depicted in Fig. 4 with those shown in Fig. 7.

For illustrative purposes, the distribution of the hysteresis losses per size category for different t and σ values is shown in Fig. 8. A slight deviation towards larger particle sizes can be observed as polydispersity increases. This feature is also depicted in Fig. 9 for the case $\sigma = 0.20$, where it is seen that at high t the hysteresis losses of the larger particles finally overcome the

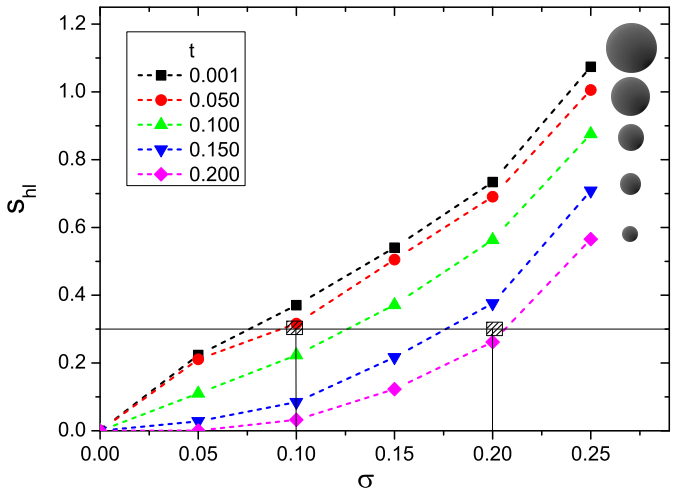

Fig. 7 Standard deviation of local hysteresis losses per particle, s_{hl}, as a function of size polydispersity σ and for different reduced temperatures t. The spheres illustrate that increasing the temperature is equivalent to choose particles with smaller sizes.

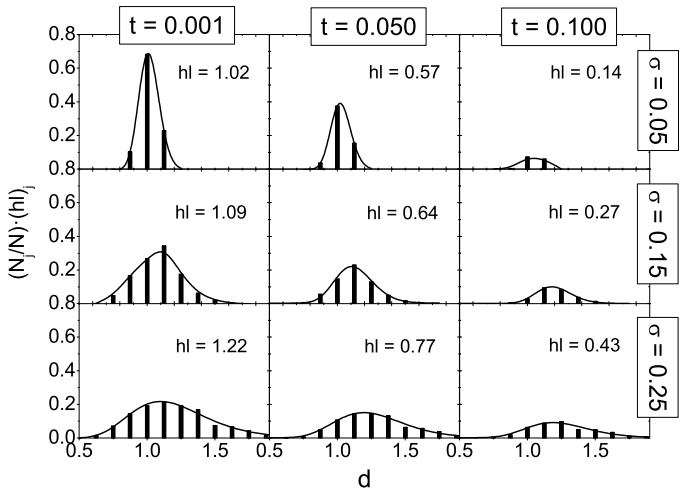

Fig. 8 Evolution of the hysteresis losses per category $(hl)_j$ as a function of the reduced temperature t and the size polydispersity σ. The corresponding values of the hysteresis losses of the entire system hl are also given in each case. Solid lines are a guide for the eye.

hl of the monodisperse case, explaining the results displayed in Fig. 4. Nevertheless, note that in both cases (monodisperse and polydisperse), the hl are very low at high t and so their efficiency for heating is reduced.

2.3 Influence of interactions

In the previous sections, non-interacting conditions were assumed in order to simplify the scenario in which to introduce the notion of global *vs.* local heat dissipation. However, such non-interacting assumption does not necessarily hold for real hyperthermia applications, where concentrated samples are used.[1] In addition, when the particles are internalized within the cells, aggregation may occur. In both cases interparticle interactions play a non-negligible role that must be taken into account. Their influence on the hyperthermia performance has been extensively studied from the global point of view,[11,16,20,37,40,48–51] but knowledge of what happens at a local level is still missing.

The general influence of interactions is known to increase the dispersion of energy barriers.[52] This means that depending on the local environment, the interactions could increase or decrease local energy barriers. In a first approximation, one could expect that for a monodisperse system at a temperature high enough as to correspond to an anhysteretic behavior, introducing interparticle dipolar interactions might increase some of the energy barriers. Depending on the strength of the coupling, this local barriers may become a heat-dissipation source. Accordingly, interactions would increase the hyperthermia performance. On the contrary, for the same non-interacting system at low temperatures where the particles dissipate the maximum, the local decrease of some energy barriers is important since they will lower the heating output.

Fig. 10 shows how dipolar interactions, varied by changing the sample concentration (volume fraction) c, and temperature modify the hysteresis losses for the monodisperse case. As expected, the hl decrease with t regardless the strength of interaction. Regarding the role of the interactions, at low t the increase of interactions decreases the hl values. The opposite occurs at high t, when we are close to the superparamagnetic behavior, where increasing interactions increase the hysteresis losses[53,54]. Note however that the influence of interactions is very complex *per se*[11] and that it becomes even more complicated in the presence of aggregations, where interaction conditions completely modify the heating response[55,56]. Such diverging behavior of interactions with temperature has been also reported in Ref. 48.

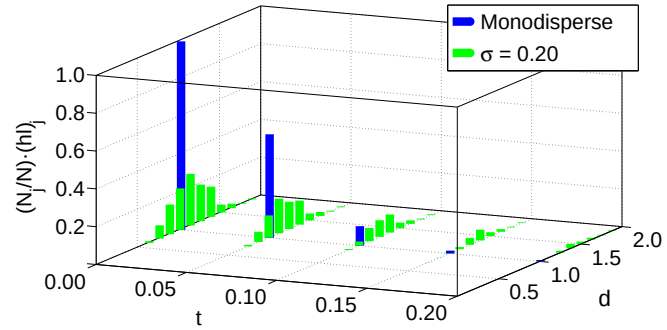

Fig. 9 Evolution of the reduced hysteresis losses per category $(hl)_j$ as a function of the reduced temperature t for a degree of polydispersity $\sigma = 0.20$. The data of the monodisperse case is also included for comparison.

Fig. 11 shows the obtained global hl values as a function of polydispersity for interacting and non-interacting conditions. In both cases the hysteresis losses increase with σ. Comparing interaction effects, at low σ and high t the hl values decrease with increasing c, whereas at high t they increase for larger c. Intermediate situations are observed depending on the combination of σ, t, and c. These results agree with the findings of Refs. 16,48. The fact that the dipolar interactions have a more pronounced effect at low t is also in agreement with Refs. 35,48.

Similar to the non-interacting case, we have analyzed the stan-

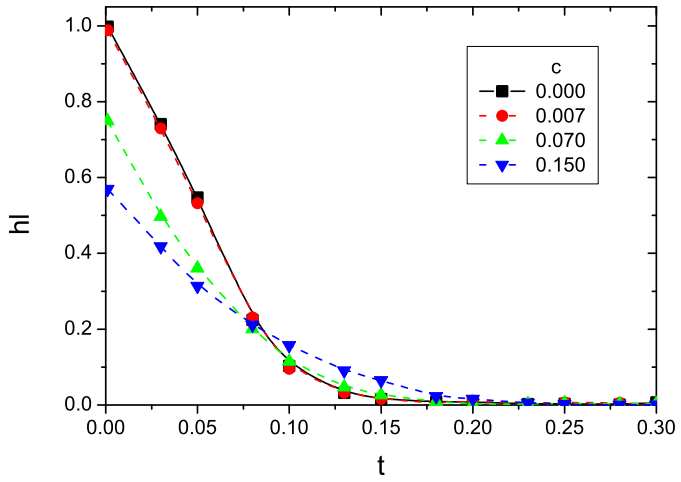

Fig. 10 Global reduced hysteresis losses hl as a function of the reduced temperature t for the monodisperse case and different sample concentrations c.

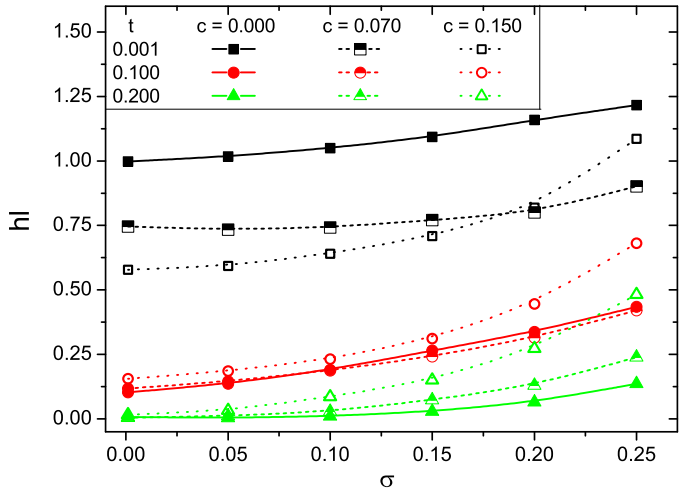

Fig. 11 Dependence on size polydispersity σ of the global reduced hysteresis losses hl for various reduced temperatures t and interaction conditions c.

dard deviation of local hl as a function of σ and t. The results are displayed in Fig. 12, together with those of the non-interacting case. The main noticeable feature in this figure is the fact that s_{hl} increases significantly with σ for strong interactions, an undesired effect for hyperthermia. For example, note that s_{hl} can achieve up to 450% for the conditions of $\sigma = 0.25$ and $c = 0.15$. Therefore, for strongly interacting systems it is crucial to use systems as monodisperse as possible.

3 Conclusions

The results reported in this work highlight the importance of taking into account size polydispersity in magnetic fluid hyperthermia studies. Even for a moderate distribution in particle diameters, the dependence of the dissipated power on the particle volume implies a broad distribution in locally released heat values. The existence of a distribution of heat dissipation spots with different performance may result highly inefficient in terms

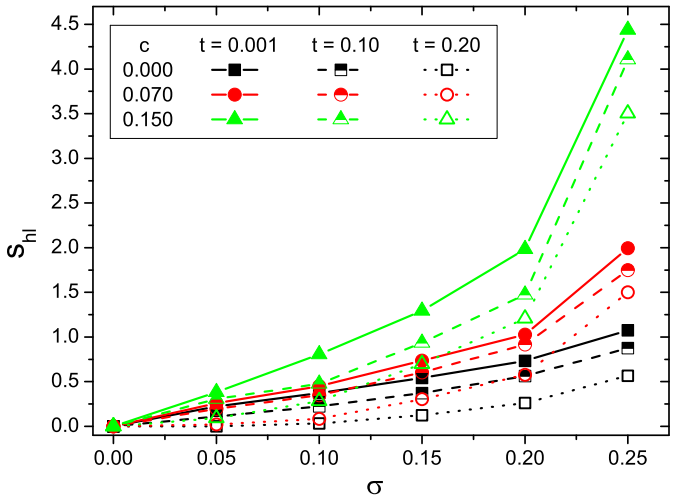

Fig. 12 Standard deviation of the local hysteresis losses s_{hl} as a function of size polydispersity σ for various reduced temperatures t and interaction conditions c, corresponding to the data plotted in Fig. 11.

of hyperthermia-based cancer treatment, with areas being overheated (risk of damage) and others remaining untreated. It is therefore crucial to keep in mind that heating and hyperthermia efficiency, though closely related, are not equivalent concepts: two different systems may have the same global heating performance, but a completely different local heat release distribution, therefore different overall hyperthermia efficiency.

Starting with the usual entire system heating considerations, we show that for a given average particle size and non-interacting conditions, the maximum achievable power of a nanoparticle system with lognormal size distribution always rises with increasing polydispersity. This analytical result, also supported by our Monte Carlo simulations, indicates that the decrease of the heating power reported in some experiments is not due to the presence of polydispersity *per se*, but must be attributed to other conditions as e.g. non-saturating field amplitudes. On the other hand, thermal fluctuations always increase the relative importance of size polydispersity, which evolves from moderate at low temperatures to dominant at high ones.

We have analyzed the distribution in local heating power as a function of size polydispersity and temperature, and also studied the role of the interparticle dipolar interactions. Using the standard deviation to characterize the local heat distribution, we obtained that s_{hl} rapidly increases with σ, whereas the temperature attenuates this growth. Our results show how the appearance of different heating spots due to size polydispersity may cause local infra/over-heating effects, clearly undesired from a clinical point of view. The quantification of the dispersion of the local heating via the standard deviation s_{hl} revealed that it can dramatically increase, achieving the 100% or even the 450% for strongly interacting systems.

Importantly, our approach to the problem in terms of dimensionless units proves to be very useful since it allows the estimation of the most suitable average particle size to achieve a more efficient hyperthermia protocol. This is simply achieved by choosing the adequate volume, for a certain K and T, so that the corre-

sponding s_{hl} values are kept below some desired value. It must be noted, however, that the way to lower the deviations in local heating is by reducing the average particle sizes which in turn lowers the heating output. A careful balance between both tendencies is therefore necessary. A promising approach in this regard may be to fine-tune interparticle interactions: despite rapidly incrementing s_{hl}, they also allow to obtain relevant heating. Interparticle dipolar interactions are thus foreseen to play a central role in the design of improved hyperthermia applications.

Note that, however, the present work has some limitations. The simulations were conducted for single-domain nanoparticles with coherent magnetization reversal. Also, full-cycle conditions were assumed, whereas in real applications field amplitude and frequency are limited. In addition, the effective uniaxial anisotropy was considered to be the same for all particles with a given size, while in a real system a distribution of anisotropy values needs to be taken into account, which is also crucial regarding field-amplitude considerations.[47] Such and other aspects need to be included in future works in order to address the specific conditions of a particular experiment. Despite the aforementioned limitations, we believe that this work provides understanding of the influence of size polydispersity in magnetic hyperthermia, emphasizing the importance of simultaneously considering the heat dissipation at both global and local levels. The results relating the clinical safety boundary requisites with the characteristics of the particles to use may constitute a promising approach for the design of more efficient hyperthermia-based cancer treatment protocols.

Acknowledgments

The authors thank the Centro de Supercomputación de Galicia (CESGA) for the computational facilities. This work was co-financed by the EU (project FEMTOSPIN, Ref. NNP3-SL-2012-281043), the Spanish MEC (FIS2010-20979-C02-02 and MAT2009-08165) and Xunta de Galicia (INCITE 08PXIB236052PR). D.S. acknowledges Xunta de Galicia (Spain) for financial support under the Plan I2C. The FPI Spanish program supported I. C-L.

References

1 D. Ortega and Q. A. Pankhurst, *Nanoscience: Volume 1: Nanostructures through Chemistry*, The Royal Society of Chemistry, 2013, vol. 1, pp. 60–88.

2 S. Dutz and R. Hergt, *Int. J. Hyperther.*, 2013, **29**, 790–800.

3 X. Wang, H. Gu and Z. Yang, *J. Magn. Magn. Mater.*, 2005, **293**, 334 – 340.

4 C. D. Kaddi, J. H. Phan and M. D. Wang, *Nanomedicine-UK*, 2013, **8**, 1323–1333.

5 M. Mahmoudi, A. Simchi and M. Imani, *J. Iran. Chem. Soc.*, 2010, **7**, S1–S27.

6 S. E. Barry, *Int. J. Hyperther.*, 2008, **24**, 451–466.

7 M. Mahmoudi, K. Azadmanesh, M. A. Shokrgozar, W. S. Journeay and S. Laurent, *Chem. Rev.*, 2011, **111**, 3407–3432.

8 G.-Q. Yi, B. Gu and L.-K. Chen, *Tumor Biol.*, 2014, **35**, 2445–2449.

9 M. Mahmoudi, S. Sant, B. Wang, S. Laurent and T. Sen, *Adv. Drug Deliver. Rev.*, 2011, **63**, 24 – 46.

10 S. Laurent, S. Dutz, U. O. Hafeli and M. Mahmoudi, *Adv. Colloid Interfac.*, 2011, **166**, 8 – 23.

11 I. Conde-Leboran, D. Baldomir, C. Martinez-Boubeta, O. Chubykalo-Fesenko, M. D. P. Morales, G. Salas, D. Cabrera, J. Camarero, F. J. Teran and D. Serantes, *J. Phys. Chem. C*, 2015, **119**, 15698–15706.

12 J. Carrey, B. Mehdaoui and M. Respaud, *J. Appl. Phys.*, 2011, **109**, 083921.

13 M. Colombo, S. Carregal-Romero, M. F. Casula, L. Gutierrez, M. P. Morales, I. B. Bohm, J. T. Heverhagen, D. Prosperi and W. J. Parak, *Chem. Soc. Rev.*, 2012, **41**, 4306–4334.

14 L. Castro, M. da Silva, A. Bakuzis and R. Miotto, *J. Magn. Magn. Mater.*, 2005, **293**, 553 – 558.

15 R. Müller, S. Dutz, A. Neeb, A. Cato and M. Zeisberger, *J. Magn. Magn. Mater.*, 2013, **328**, 80 – 85.

16 N. L. Tran and H. H. Tran, *J. Non-Cryst. Solids*, 2011, **357**, 996 – 999.

17 V. Russier, C. de Montferrand, Y. Lalatonne and L. Motte, *J. Appl. Phys.*, 2012, **112**, 073926.

18 G. H. Jaffari, T. Ekiert, K. Unruh and S. I. Shah, *Mater. Sci. Eng. B*, 2012, **177**, 935 – 941.

19 G. Salas, C. Casado, F. J. Teran, R. Miranda, C. J. Serna and M. P. Morales, *J. Mater. Chem.*, 2012, **22**, 21065–21075.

20 C. Haase and U. Nowak, *Phys. Rev. B*, 2012, **85**, 045435.

21 R. Rosensweig, *J. Magn. Magn. Mater.*, 2002, **252**, 370 – 374.

22 M. Gonzales-Weimuller, M. Zeisberger and K. M. Krishnan, *J. Magn. Magn. Mater.*, 2009, **321**, 1947 – 1950.

23 A. P. Khandhar, R. M. Ferguson and K. M. Krishnan, *J. Appl. Phys.*, 2011, **109**, 07B310.

24 M. Jeun, S. Bae, A. Tomitaka, Y. Takemura, K. H. Park, S. H. Paek and K.-W. Chung, *Appl. Phys. Lett.*, 2009, **95**, 082501.

25 M. Creixell, A. C. Bohórquez, M. Torres-Lugo and C. Rinaldi, *ACS Nano*, 2011, **5**, 7124–7129.

26 L. Asín, M. Ibarra, A. Tres and G. Goya, *Pharmaceut. Res.*, 2012, **29**, 1319–1327.

27 V. Grazú, A. Silber, M. Moros, L. Asin, T. Torres, C. Marquina, M. Ibarra and G. Goya, *Int. J. Nanomedicine*, 2012, **7**, 5351–5360.

28 A. Villanueva, P. de la Presa, J. M. Alonso, T. Rueda, A. Martínez, P. Crespo, M. P. Morales, M. A. Gonzalez-Fernandez, J. Valdés and G. Rivero, *J. Phys. Chem. C*, 2010, **114**, 1976–1981.

29 F. Henrich, H. Rahn and S. Odenbach, *J. Magn. Magn. Mater.*, 2014, **351**, 1 – 7.

30 W. Andrä, C. d'Ambly, R. Hergt, I. Hilger and W. Kaiser, *J. Magn. Magn. Mater.*, 1999, **194**, 197 – 203.

31 J. T. Dias, M. Moros, P. del Pino, S. Rivera, V. Grazú and J. M. de la Fuente, *Angew. Chem. Int. Edit.*, 2013, **52**, 11526–11529.

32 A. Riedinger, P. Guardia, A. Curcio, M. A. Garcia, R. Cingolani, L. Manna and T. Pellegrino, *Nano Lett.*, 2013, **13**, 2399–2406.

33 G. Kucsko, P. Maurer, N. Y. Yao, M. Kubo, H. Noh, P. Lo,

H. Park and M. D. Lukin, *Nature*, 2013, **500**, 54–58.
34 P. de la Presa, Y. Luengo, M. M, R. Costo, M. P. Morales and A. Hernando, *J. Phys. Chem. C*, 2012, **116**, 25602–25610.
35 R. Zysler, D. Fiorani and A. Testa, *J. Magn. Magn. Mater.*, 2001, **224**, 5 – 11.
36 E. Garaio, O. Sandre, J.-M. Collantes, J. A. Garcia, S. Mornet and F. Plazaola, *Nanotechnology*, 2015, **26**, 015704.
37 C. Martinez-Boubeta, K. Simeonidis, D. Serantes, I. Conde-Leborán, I. Kazakis, G. Stefanou, L. Peña, R. Galceran, L. Balcells, C. Monty, D. Baldomir, M. Mitrakas and M. Angelakeris, *Adv. Funct. Mater.*, 2012, **22**, 3737–3744.
38 B. Mehdaoui, A. Meffre, J. Carrey, S. Lachaize, L.-M. Lacroix, M. Gougeon, B. Chaudret and M. Respaud, *Adv. Funct. Mat.*, 2011, **21**, 4573–4581.
39 M. J. Howenstein and K. T. Sato, Seminars in interventional radiology, 2010, pp. 285–295.
40 D. Serantes, D. Baldomir, C. Martinez-Boubeta, K. Simeonidis, M. Angelakeris, E. Natividad, M. Castro, A. Mediano, D.-X. Chen, A. Sanchez, L. Balcells and B. Martínez, *J. Appl. Phys.*, 2010, **108**, 073918.
41 C. Martinez-Boubeta, K. Simeonidis, A. Makridis, M. Angelakeris, O. Iglesias, P. Guardia, A. Cabot, L. Yedra, S. Estradé, F. Peiró *et al.*, *Sci. Rep.*, 2013, **3**,.
42 S. Dutz, M. Kettering, I. Hilger, R. Müller and M. Zeisberger, *Nanotechnology*, 2011, **22**, 265102.
43 R. D. Corato, A. Espinosa, L. Lartigue, M. Tharaud, S. Chat, T. Pellegrino, C. Ménager, F. Gazeau and C. Wilhelm, *Biomaterials*, 2014, **35**, 6400 – 6411.
44 N. A. Usov and B. Y. Liubimov, *J. Appl. Phys.*, 2012, **112**, 023901.
45 H. Nemala, J. S. Thakur, V. M. Naik, P. P. Vaishnava, G. Lawes and R. Naik, *J. Appl. Phys.*, 2014, **116**, 034309.
46 S. Ruta, R. Chantrell and O. Hovorka, *Sci. Rep.*, 2015, **5**,.
47 G. Vallejo-Fernandez and K. O'Grady, *Appl. Phys. Lett.*, 2013, **103**, 142417.
48 G. T. Landi, *Phys. Rev. B*, 2014, **89**, 014403.
49 B. Mehdaoui, R. P. Tan, A. Meffre, J. Carrey, S. Lachaize, B. Chaudret and M. Respaud, *Phys. Rev. B*, 2013, **87**, 174419.
50 L. C. Branquinho, M. S. Carrião, A. S. Costa, N. Zufelato, M. H. Sousa, R. Miotto, R. Ivkov and A. F. Bakuzis, *Sci. Rep.*, 2013, **3**,.
51 G. Salas, J. Camarero, D. Cabrera, H. Takacs, M. Varela, R. Ludwig, H. Dähring, I. Hilger, R. Miranda, M. P. Morales and F. J. Teran, *J. Phys. Chem. C*, 2014, **118**, 19985–19994.
52 O. Chubykalo-Fesenko and R. Chantrell, *J. Appl. Phys.*, 2005, **97**, 10J315.
53 A. Cervadoro, C. Giverso, R. Pande, S. Sarangi, L. Preziosi, J. Wosik, A. Brazdeikis and P. Decuzzi, *PloS One*, 2013, **8**, e57332.
54 T. Sadhukha, L. Niu, T. S. Wiedmann and J. Panyam, *Mol. Pharm.*, 2013, **10**, 1432–1441.
55 M. Sadat, R. Patel, J. Sookoor, S. L. Bud'ko, R. C. Ewing, J. Zhang, H. Xu, Y. Wang, G. M. Pauletti, D. B. Mast and S. Donglu, *Mat. Sci. Eng.: C*, 2014, **42**, 52–63.
56 D. Serantes, K. Simeonidis, M. Angelakeris, O. Chubykalo-Fesenko, M. Marciello, M. del Puerto Morales, D. Baldomir and C. Martinez-Boubeta, *J. Phys. Chem. C*, 2014, **118**, 5927–5934.